HHS Public Access

Author manuscript

Mol Imaging Biol. Author manuscript; available in PMC 2017 January 24.

Published in final edited form as:

Mol Imaging Biol. 2016 June ; 18(3): 411–419. doi:10.1007/s11307-016-0957-6.

PSMA-Based [^{18}F]DCFPyL PET/CT Is Superior to Conventional Imaging for Lesion Detection in Patients with Metastatic Prostate Cancer

Steven P. Rowe[1], **Katarzyna J. Macura**[1], **Esther Mena**[1], **Amanda L. Blackford**[2], **Rosa Nadal**[2], **Emmanuel S. Antonarakis**[2], **Mario Eisenberger**[2], **Michael Carducci**[2], **Hong Fan**[1], **Robert F. Dannals**[1], **Ying Chen**[1], **Ronnie C. Mease**[1], **Zsolt Szabo**[1], **Martin G. Pomper**[1], and **Steve Y. Cho**[1,3]

[1]The Russell H. Morgan Department of Radiology and Radiological Science, Johns Hopkins Medical Institutions, Baltimore, MD, USA

[2]Department of Oncology in the Sidney Kimmel Comprehensive Cancer Center, Johns Hopkins Medical Institutions, Baltimore, MD, USA

[3]Department of Radiology, University of Wisconsin-Madison, 1111 Highland Avenue, WIMR1 Rm 7139, Madison, 53593, WI, USA

Abstract

Purpose—Current standard of care conventional imaging modalities (CIM) such as X-ray computed tomography (CT) and bone scan can be limited for detection of metastatic prostate cancer and therefore improved imaging methods are an unmet clinical need. We evaluated the utility of a novel second-generation low molecular weight radiofluorinated prostate-specific membrane antigen (PSMA)-targeted positron emission tomography (PET) radiotracer, [^{18}F]DCFPyL, in patients with metastatic prostate cancer.

Procedures—Nine patients with suspected prostate cancer recurrence, eight with CIM evidence of metastatic prostate cancer and one with biochemical recurrence, were imaged with [^{18}F]DCFPyL PET/CT. Eight of the patients had contemporaneous CIM for comparison. A lesion-by-lesion comparison of the detection of suspected sites of metastatic prostate cancer was carried out between PET and CIM. Statistical analysis for estimated proportions of inter-modality agreement for detection of metastatic disease was calculated accounting for intra-patient correlation using general estimating equation (GEE) intercept-only regression models.

Results—One hundred thirty-nine sites of PET positive [^{18}F]DCFPyL uptake (138 definite, 1 equivocal) for metastatic disease were detected in the eight patients with available comparison CIM. By contrast, only 45 lesions were identified on CIM (30 definite, 15 equivocal). When

Correspondence to: Steve Cho; scho@uwhealth.org.

Electronic supplementary material The online version of this article (doi:10.1007/s11307-016-0957-6) contains supplementary material, which is available to authorized users.

Conflict of Interest

MGP, RCM, and YC are co-inventors on a US Patent covering [^{18}F]DCFPyL and as such are entitled to a portion of any licensing fees and royalties generated by this technology. This arrangement has been reviewed and approved by the Johns Hopkins University in accordance with its conflict of interest policies.

lesions were negative or equivocal on CIM, it was estimated that a large portion of these lesions or 0.72 (95 % confidence interval (CI) 0.55–0.84) would be positive on [^{18}F]DCFPyL PET. Conversely, of those lesions negative or equivocal on [^{18}F]DCFPyL PET, it was estimated that only a very small proportion or 0.03 (95 % CI 0.01–0.07) would be positive on CIM. Delayed 2-h-post-injection time point PET yielded higher tumor radiotracer uptake and higher tumor-to-background ratios than an earlier 1-h-post-injection time point.

Conclusions—A novel PSMA-targeted PET radiotracer, [^{18}F]DCFPyL, was able to a large number of suspected sites of prostate cancer, many of which were occult or equivocal by CIM. This study provides strong preliminary evidence for the use of this second-generation PSMA-targeted PET radiotracer for detection of metastatic prostate cancer and lends further support for the importance of PSMA-targeted PET imaging in prostate cancer.

Keywords

Metastatic prostate cancer; Prostate-specific membrane antigen (PSMA); PET/CT; [^{18}F]DCFPyL; Computed tomography (CT); Bone scan

Introduction

Prostate cancer is the most common malignancy diagnosed in men in the USA [1]. Currently, men with known or suspected metastatic prostate cancer are most commonly evaluated and followed using the conventional imaging modalities (CIM) of contrast-enhanced computed tomography (CECT) of the chest, abdomen, and pelvis and [^{99}Tc]methylene diphosphonate bone scan (BS). Though these modalities are able to detect a large number of metastatic prostate cancer sites, they still suffer from limitations including regions of degenerative bone change that can appear as sclerotic lesions on CECT and have corresponding uptake on BS; lytic or infiltrative bone metastases that generate scant surrounding bony reaction and have no appreciable sclerosis on CECT or uptake on BS; and small lymph nodes (less than 1 cm short axis) that are not able to be definitively characterized as disease involved on CECT.

Within the context of these limitations, it should be noted that clinically applied positron emission tomography (PET) such as 2-deoxy-2-[^{18}F]fluoro-D-glucose ([^{18}F]FDG) and sodium [^{18}F]fluoride ([^{18}F]NaF) lack either sensitivity ([^{18}F]FDG) or specificity ([^{18}F]NaF) for metastatic prostate cancer detection in some circumstances [2]. A great deal of effort has therefore been expended in the development of new PET functional imaging agents that might allow for improved sensitivity and specificity in the detection of metastatic prostate cancer. Among these are compounds that localize in areas of high fatty acid synthesis ([^{11}C]choline, [^{18}F]fluorocholine, and [^{11}C]acetate) or amino acid transport ([^{18}F]FACBC) [3–11]. Examples of new PET agents also include those targeting gastrin-releasing peptide (GRP) [12, 13], glutamine [14, 15], and the prostate-specific membrane antigen (PSMA) [16–22].

PSMA is an attractive target given that is expressed on the cell surface of the vast majority of prostate cancers [23, 24]. Levels of PSMA expression are correlated with tumor aggressiveness including metastatic potential [25–29]. Our group has previously published

data on detecting primary and metastatic prostate cancer using a first-in-class radiofluorinated small molecule inhibitor of PSMA, N-[N-[(*S*)-1,3-dicarboxypropyl]carbamoyl]-4-[^{18}F]fluorobenzyl-L-cysteine ([^{18}F]DCFBC) [16, 30, 31]. Although [^{18}F]DCFBC demonstrated an ability to accurately detect high grade primary prostate cancer and was superior to CIM in the detection of metastatic prostate cancer, that radiotracer possessed some features that could potentially be improved through further refinements in the chemical structure. As a result, we have undertaken the synthesis and pre-clinical evaluation of a second-generation radiofluorinated inhibitor of PSMA, 2-(3-{1-carboxy-5-[(6-[^{18}F]fluoro-pyridine-3-carbonyl)-amino]-pentyl}-ureido)-pentanedioic acid ([^{18}F]DCFPyL, Supplementary Fig. 1) [32]. As described in a first-in-human biodistribution and dosimetry publication, [^{18}F]DCFPyL is notable for markedly reduced blood pool activity in comparison to [^{18}F]DCFBC with corresponding overall higher uptake in foci of presumed metastatic prostate cancer [17]. Here, we describe a lesion-by-lesion analysis of the ability of [^{18}F]DCFPyL to detect suspected sites of metastatic disease in comparison to CIM.

Materials and Methods

Patient Population and Selection

Approval of this prospective study was granted by our hospital's Institutional Review Board (IRB) and all patients were imaged under the auspices of a Food and Drug Administration exploratory investigation new drug application (eIND 108943), ClinicalTrials.gov Identifier:NCT02151760. The patients included in this manuscript are the same cohort that were previously described in our group's prior first-in-man publication on the biodistribution and dosimetry of [^{18}F]DCFPyL [17]. Written, informed consent was obtained from all participants. Important inclusion criteria for this study included histologic confirmation of prostate cancer, radiologic evidence of new or progressive metastatic prostate cancer on another imaging modality (CECT, BS, magnetic resonance imaging (MRI), ultrasound, [^{18}F]FDG PET/CT, or [^{18}F]NaF PET/CT), and a prostate-specific antigen (PSA) serum level of at least 1 ng/ml. Eight out of the nine imaged patients met all of the inclusion criteria, though a single patient with a PSA level of 0.1 ng/ml on androgen deprivation therapy (ADT) and with no evidence of disease on CECT, BS, or pelvic MRI but with high clinical suspicion for pelvic disease recurrence was imaged following an IRB-approved planned protocol deviation.

Important exclusion criteria for this study included low Karnovsky performance status (<60); prostate brachytherapy implants; treatment with an investigational drug, biologic, or device within 30 days prior to trial enrollment; administration of another radioisotope within five physical half-lives of trial enrollment; radiation or chemotherapy within 2 weeks prior to trial enrollment; or prior history of another malignancy other than skin basal cell carcinoma. Additionally, patients could not have serum creatinine or bilirubin >3 times the upper limit of normal or have liver transaminases >5 times the upper limit of normal.

Nine patients were prospectively enrolled between July and September 2014. Seven of those patients had complete CIM including CECT of the chest, abdomen, and pelvis and BS; one

patient had CECT of the abdomen and pelvis and BS; and one patient had no recent CIM. Selected demographic and clinical information from the patients is included in Table 1.

Radiochemistry

The [^{18}F]DCFPyL precursor (*S*)-di-*tert*-butyl-1,2-(3-((*S*)-6-amino-1-(*tert*-butoxy)-1-oxohexan-2-yl)-ureido)-pentanedioate formate salt was manufactured using current good manufacturing practices as has been previously reported [32]. Coupling to the radiolabeled prosthetic group 2,3,5,6-tetrafluorophenyl-6-[^{18}F]fluoronicotinate was then performed. Acid hydrolysis yielded [^{18}F]DCFPyL. Average yield, specific activity, and radiochemical purity are as reported in our companion biodistribution and dosimetry. The administered specific activity range was 85.8–141.0 MBq/nmol (2.32–3.81 Ci/μmol).

PET/CT Protocol

Though the effect of the fasting state on [^{18}F]DCFPyL uptake is unknown, per our typical clinical PET protocol we asked patients remain *nil per os* (except for water and some medications) for at least 6 h prior to radiotracer injection. In particular, given that folate is a low-affinity ligand for PSMA and with theoretical potential to decrease binding of [^{18}F]DCFPyL to PSMA [23, 33, 34], patients were specifically instructed to avoid multivitamins and folate supplements on the day of the examination.

The [^{18}F]DCFPyL PET/CT acquisition was performed on a Discovery DRX PET/CT scanner (GE Healthcare, Waukesha, WI) operating in 3D emission mode with CT-derived attenuation correction. Initially, a whole body (WB, from the top of the skull through the mid-thighs) CT was obtained (120 kVp, 80 mA maximum (auto-adjusting)). Subsequently, a bolus injection of 9 mCi (331 MBq) or less of [^{18}F]DCFPyL was administered through a peripheral IV catheter. A series of four sequential PET acquisitions were then obtained (labeled PET1 through PET4) beginning immediately after injection, followed by the patient voiding his bladder, followed by a second CT scan and additional PET acquisition (PET5). For PET1, imaging was performed for 1 min per bed position; for PET 2, 2 min per bed position; for PET3 and PET4, 4 min per bed position; and for PET5, 4 min per bed position. The PET4 acquisition began at approximately 60 min post-injection, depending on the patient height due to number of bed positions, and the PET5 acquisition always began at 120 min post-injection. The acquired PET images were reconstructed using a standard clinical ordered subset expectation maximization (OSEM) algorithm.

Image Analysis

Based on information in our group's prior first-in-man manuscript [17], the PET4 and PET5 imaging time points demonstrated high tumor-to-background ratios and the lesion-by-lesion analysis was carried out based on those acquisitions. The PET1-PET3 acquisitions were not further analyzed. [^{18}F]DCFPyL PET/CT images were viewed on a Mirada Medical workstation (Mirada Medical, Oxford, UK). Measurements of background uptake were obtained as mean standardized uptake value (SUV_{mean}) from the ascending aorta (blood pool), liver, a non-disease-involved vertebral body, and the right gluteus musculature. Two experienced nuclear medicine readers (SPR and SYC) examined the PET images and provided a consensus read on the location of abnormal uptake suspicious or equivocal for

sites of metastatic or primary prostate cancer (defined as visually conspicuous above nearby background uptake at a site outside of the normal biodistribution of the radiotracer). Suspected sites of metastases or tumor on DCFPyL PET were quantified using maximum SUV (SUV_{max}). Correlative BS images were also reviewed on the Mirada by two experienced readers (SPR and SYC), again with consensus reached as to any sites felt to be positive or equivocal for disease involvement. Correlative CECT images were reviewed by a single expert reviewer (KJM).

Statistical Analysis

Estimates of the proportion of agreement in lesion detection between [^{18}F]DCFPyL PET, CECT, BS, and combined CIM were arrived at through general estimating equation (GEE) intercept-only regression models and an exchangeable correlation structure. This methodology accounts for intra-patient correlation in the scenario of multiple lesions being present in a single patient. Estimated proportion of agreement was also determined between the modalities based on type of lesion (lymph node, bone, or prostate/prostate bed). Average within-patient differences in SUV parameters were modeled using the same GEE approach and results are reported with model-based p values. Analyses were completed with R version 3.1.2 [35].

Results

An example maximum intensity projection (MIP) image from a patient with numerous [^{18}F]DCFPyL-avid lymph node and bone lesions at the PET5 time point is shown in Fig. 1. Normal radiotracer uptake within the lacrimal and salivary glands, liver, kidneys, and urinary bladder is noted. Both the PET4 and PET5 time points were considered for a lesion-by-lesion analysis. Indeed, the vast majority of [^{18}F]DCFPyL-avid lesions were visible at both time points. However, a total of eight sites of mild subtle focal bone uptake were identified only on the PET5 images, with an example shown in Fig. 2. Furthermore, the overall maximum standardized uptake values (SUV_{max}) normalized to lean body mass for the tumors demonstrated a statistically significant increase between approximately 1 and 2 h post-injection on the PET4 and PET5 scans, respectively, in an aggregate of all sites of abnormal [^{18}F]DCFPyL uptake ($p = 0.01$), for lymph node uptake ($p = 0.03$) and for bone uptake ($p = 0.01$), and a trend towards increased uptake on PET5 for other sites (prostate, prostate bed, peri-prostatic tissue, and other soft tissue lesions) (Fig. 3). In comparison, measures of background [^{18}F]DCFPyL uptake in the mediastinal blood pool, gluteus muscle, and vertebral bodies showed a statistically significant trend towards decreasing uptake between PET4 and PET5, with statistically increased mild uptake in the liver (Supplementary Fig. 2). Given these findings, all further analysis for metastatic detection on [^{18}F]DCFPyL PET was carried out on the data from the PET5 time point PET/CT data.

For the nine patients imaged in this study, a total of 190 lesions were identified on at least one modality. Out of those lesions, 171 were identified as foci of abnormal [^{18}F]DCFPyL uptake during the central review of the PET5 images (the median number of [^{18}F]DCFPyL-avid lesions per patient was 8, with a range from 1 through 77). Pathologic proof of metastatic prostate cancer is only available from one lesion (a rectal wall metastasis in

patient 3); therefore, these sites of increased radiotracer uptake will generally be referred to as sites of putative or presumptive metastatic disease.

Of the lesions on PET5, 170 were considered definite and 1 lesion was considered to be equivocal; this high degree of certainty in lesion detection by the reviewers is likely related to the generally high tumor-to-background uptake demonstrated by [^{18}F]DCFPyL-avid lesions. Excluding the patient for whom no comparison CIM was available, there were 138 definite [^{18}F]DCFPyL positive lesions and 1 equivocal lesion. In comparison, for the same patient cohort, CECT identified 31 lesions (20 definite and 11 equivocal), BS identified 18 lesions (13 definite and 5 equivocal), and combined CIM identified 45 lesions (30 definite and 15 equivocal). Additional details of lesion detection by modality for the eight patients with comparison CIM are included in Table 2.

[^{18}F]DCFPyL was able to detect sites of putative prostate cancer in bone, lymph nodes, and the prostate bed and surrounding tissues. One of the patients imaged in this study had never undergone prostatectomy, and an intensely [^{18}F]DCFPyL-avid lesion was also seen in his in situ prostate. In all, 78 lesions were detected in bone, 95 were detected in lymph nodes, and 11 were detected in the prostate, prostate bed, or peri-prostatic tissues.

Given the wide numerical range of lesions detected among these patients, a GEE regression analysis was performed in order to take into account intra-patient clustering effects as described in the materials and methods section [36]. Based on this analysis, it was estimated that a proportion of 0.54 (95 % CI 0.34–0.72) of the lesions that were negative or equivocal on CIM would be positive on [^{18}F]DCFPyL PET. In contradistinction, it was estimated that a proportion of only 0.03 (95 % CI 0.01–0.08) of lesions that were negative or equivocal on [^{18}F]DCFPyL PET would be positive on CIM. Additional estimated proportions of inter-modality agreement are presented in Table 3. Lesions that were positive on CIM but negative or equivocal on [^{18}F]DCFPyL PET were two densely sclerotic lesions on CECT and a BS lesion; 10 additional bone lesions that were negative on [^{18}F]DCFPyL PET were equivocal on CECT and/or BS.

Similar to our observations with our first-generation compound, we found that [^{18}F]DCFPyL is able to identify multiple different types of lesions that are not well evaluated with CIM. One of these lesion types is the infiltrative or lytic bone metastasis. Such metastatic foci are notable for a lack of surrounding bony reaction/sclerosis, and as such are visually difficult to detect on CECT and can be ostensibly invisible on BS. An example of such a lesion is shown in Fig. 4, with no evidence of a significant abnormality on either CECT or planar BS, but with intense [^{18}F]DCFPyL uptake.

Another group of lesions that is well evaluated by [^{18}F]DCFPyL is small lymph nodes. While the high spatial resolution afforded by CECT certainly allows for the sensitive identification of small lymph nodes, specificity for metastatic disease involvement can be limited and often relies on simple measures such as a size threshold (for example, the 1-cm short axis cutoff that is used in RECIST to determine if a lymph node is disease-involved). We encountered a number of examples of lymph nodes measuring much less than 1 cm in short axis that were intensely [^{18}F]DCFPyL-avid, with an example shown in Fig. 5.

We also note that intense [^{18}F]DCFPyL uptake was present in the pelvic/peri-prostatic tissues of several patients. This can be an intrinsically difficult region to assess with CECT due to the limited soft tissue contrast available with that modality. MRI can effectively evaluate the pelvis both pre-prostatectomy and post-prostatectomy, though in the only patient in our study with a comparison MRI, the MRI demonstrated no evidence of disease recurrence whereas the [^{18}F]DCFPyL PET showed elevated radiotracer uptake in the rectal/peri-rectal soft tissues (Fig. 6). The patient underwent a rectal exam and was found to have a palpable nodule along the left anterior rectum; a subsequent biopsy proved the presence of PSMA-positive prostate cancer.

Discussion

PSMA-based PET/CT is a rapidly emerging and highly promising means of imaging metastatic prostate cancer [16–22]. Both our work with radiofluorinated low molecular weight compounds as well as work with other groups with Zirconium-89 and Gallium-68 PSMA agents has highlighted this potential. Though a great deal of work remains to fully validate PSMA as a new clinical standard for the imaging of prostate cancer, the growing body of data suggesting superiority to CIM is promising. Indeed, in this study, we encountered a number of lesions, including the above-noted non-sclerotic bone foci and small lymph nodes, for which PSMA-based PET/CT with [^{18}F]DCFPyL revealed unsuspected sites of putative metastatic prostate cancer.

While our first-generation PSMA-targeted radiotracer, [^{18}F]DCFBC, demonstrated persistently high blood pool activity, [^{18}F]DCFPyL clears rapidly from the blood stream, potentially allowing for more confident identification of subtle metastatic lesions in such locations as the retroperitoneum and pelvic sidewall. Additionally, the concentration of the [^{18}F]DCFPyL within sites of presumed prostate cancer metastasis is visually much higher than the corresponding uptake with [^{18}F]DCFBC, though direct comparison is difficult as we have not imaged the same patient with both radiotracers within a short time period and we do not know the level of PSMA expression within individual lesions. Supplementary Fig. 3a is a MIP from a patient imaged with [^{18}F]DCFBC and can be compared to Supplementary Fig. 3b which is representative of a patient imaged with [^{18}F]DCFPyL.

It is worth noting that a small number of lesions become visible between the PET4 and PET5 acquisitions. This concords with the observations that tumoral uptake, as measured by SUV_{max}, and tumor-to-background ratios increased between PET4 and PET5 (Fig. 3 and Supplementary Fig. 2). All eight of the sites of putative disease that became apparent on PET5 alone were bone lesions with relatively subtle uptake. An example is shown in Fig. 2. It is likely that most patients with known metastatic prostate cancer being followed for disease progression or response to therapy would be well evaluated at 1 h post-injection (approximately the time of PET4), a time frame that would very conveniently fit into the work flow at most PET sites given the common practice of imaging FDG at that same time point. However, for selected patients, such as those with a low PSA in the context of a new biochemical recurrence, more delayed imaging at 2 h post-injection (i.e., the PET5 time point) may more definitively evaluate their disease status. Further evaluation of

[^{18}F]DCFPyL in such patient populations will help to determine the highest yielding and most convenient imaging protocol.

Emerging Gallium-68 PSMA PET agents have also been reported to have greatly improved detection of metastatic lesions in patients with biochemical recurrence after prostatectomy compared to conventional imaging [37] and [^{18}F]fluoromethylcholine [38, 39]. An initial report of the first comparison of PSMA-based prostate cancer imaging between [^{18}F]DCFPyL to [^{68}Ga]PSMA-HBED-CC demonstrated higher PET tumor-to-background ratio with [^{18}F]DCFPyL and detection of additional metastases in 3 of 14 patients using [^{18}F]DCFPyL [40]. It will need to be determined in futures studies if there is a clinically significant difference between either Fluorine-18 or Gallium-68 PSMA agents for detection of metastatic prostate cancer, with the advantage of Gallium-68 including easier radiochemistry and generator produced Gallium-68 without requirement for an on-site cyclotron and potential integration to theranostic applications. The advantages to F-18 PSMA agents include ease of distribution utilizing pre-existing networks for FDG and improved spatial resolution and theoretically more accurate quantitation inherent in the shorter positron range and higher positron yield of F-18 versus Ga-68 [41].

Potential limitations of this study merit comment. First, the design of this study did not specifically call for contemporaneous CIM. Thus, one of the imaged patients, who had multiple bone and lymph node lesions with intense [^{18}F]DCFPyL uptake, was excluded from the lesion-by-lesion analysis on the basis of having no recent CIM. A second patient, indeed the patient in our study with the most [^{18}F]DCFPyL-avid lesions, lacked a recent diagnostic chest CT. Future studies validating [^{18}F]DCFPyL may incorporate a specific timetable for imaging with CIM in order to assure complete comparisons are possible. Additionally, one patient had 77 lesions identified on [^{18}F]DCFPyL imaging, more than all of the other patients combined—as such, even with intra-patient clustering effects partially corrected by GEE regression analysis, the results from that patient would disproportionately affect the analysis. Further, an important limitation of any study such as this is the impracticality of obtaining pathologic proof of many of the lesions identified. Indeed, only one lesion imaged in this study was biopsy proven to be prostate cancer. As such, the concept that the [^{18}F]DCFPyL-avid lesions are PSMA-expressing foci of prostate cancer remains an unproven, though reasonable, supposition.

Lastly, this study was designed as a pilot trial to assess the feasibility of imaging metastatic prostate cancer with [^{18}F]DCFPyL. Thus, a relatively small number of patients were imaged. While the small number of patients is somewhat offset by the large number of discreet lesions and the performance of a lesion-by-lesion analysis, larger patient trials are certainly needed to validate these initial results. Larger trials would also allow careful analysis of what role clinical parameters, such as castrate-sensitive or castrate-resistant status, may play in [^{18}F]DCFPyL uptake.

Conclusion

PSMA-based PET/CT with the second-generation radiotracer [^{18}F]DCFPyL was able to identify a large number of putative sites of metastatic prostate cancer that were occult or

indeterminate with conventional imaging. PET imaging at 2-h post-injection may improve tumor lesion detection compared to earlier time-point imaging but requires further verification. If these results are validated in larger prospective trials, [^{18}F]DCFPyL PET/CT may ultimately prove a more reliable means of identifying and following metastatic prostate cancer than currently available imaging methods.

Supplementary Material

Refer to Web version on PubMed Central for supplementary material.

Acknowledgments

We would like to thank funding from the Prostate Cancer Foundation-Young Investigator Award, CA134675, CA184288, CA103175, CA183031. We thank Akimosa Jeffrey-Kwanisai and Yavette Morton for providing clinical coordination of this trial.

References

1. Siegel R, Ma J, Zou Z, Jemal A. Cancer statistics, 2014. Cancer J Clin. 2014; 64:9–29.
2. Jadvar H. Prostate cancer: PET with 18F-FDG, 18F- or 11C-acetate, and 18F- or 11C-choline. J Nucl Med. 2011; 52:81–89. [PubMed: 21149473]
3. Bauman G, Belhocine T, Kovacs M, Ward A, Beheshti M, Rachinsky I. 18F-fluorocholine for prostate cancer imaging: a systematic review of the literature. Prostate Cancer Prostatic Dis. 2012; 15:45–55. [PubMed: 21844889]
4. Beheshti M, Treglia G, Zakavi SR, et al. Application of 11C-acetate positron-emission tomography (PET) imaging in prostate cancer: systematic review and meta-analysis of the literature. Br J Urol Int. 2013; doi: 10.1111/bju.12279
5. Evangelista L, Guttilla A, Zattoni F, Muzzio PC. Utility of choline positron emission tomography/computed tomography for lymph node involvement identification in intermediate- to high-risk prostate cancer: a systematic literature review and meta-analysis. Eur Urol. 2013; 63:1040–1048. [PubMed: 23036576]
6. Evangelista L, Zattoni F, Guttilla A, Saladini G, Colletti PM, Rubello D. Choline PET or PET/CT and biochemical relapse of prostate cancer: a systematic review and meta-analysis. Clin Nucl Med. 2013; 38:305–314. [PubMed: 23486334]
7. Fuccio C, Rubello D, Castellucci P, Marzola MC, Fanti S. Choline PET/CT for prostate cancer: main clinical applications. Eur J Radiol. 2011; 80:e50–e56. [PubMed: 20800404]
8. Mertens K, Slaets D, Lambert B, Acou M, De Vos F, Goethals I. PET with (18)F-labelled choline-based tracers for tumour imaging: a review of the literature. Eur J Nucl Med Mol Imaging. 2010; 37:2188–2193. [PubMed: 20544193]
9. Umbehr MH, Muntener M, Hany T, Sulser T, Bachmann LM. The role of 11C-choline and 18F-fluorocholine positron emission tomography (PET) and PET/CT in prostate cancer: a systematic review and meta-analysis. Eur Urol. 2013; 64:106–117. [PubMed: 23628493]
10. Schuster DM, Votaw JR, Nieh PT, et al. Initial experience with the radiotracer anti-1-amino-3-18F-fluorocyclobutane-1-carboxylic acid with PET/CT in prostate carcinoma. J Nucl Med. 2007; 48:56–63. [PubMed: 17204699]
11. Schuster DM, Savir-Baruch B, Nieh PT, et al. Detection of recurrent prostate carcinoma with anti-1-amino-3-18F-fluorocyclobutane-1-carboxylic acid PET/CT and 111In-capromab pendetide SPECT/CT. Radiology. 2011; 259:852–861. [PubMed: 21493787]
12. Wieser G, Mansi R, Grosu AL, et al. Positron emission tomography (PET) imaging of prostate cancer with a gastrin releasing peptide receptor antagonist—from mice to men. Theranostics. 2014; 4:412–419. [PubMed: 24578724]

13. Sah BR, Burger IA, Schibli R, et al. Dosimetry and first clinical evaluation of the new 18F-radiolabeled bombesin analogue BAY 864367 in patients with prostate cancer. J Nucl Med. 2015; 56:372–378. [PubMed: 25678494]
14. Venneti S, Dunphy MP, Zhang H, et al. Glutamine-based PET imaging facilitates enhanced metabolic evaluation of gliomas in vivo. Sci Transl Med. 2015; 7:274ra17.
15. Huang C, McConathy J. Fluorine-18 labeled amino acids for oncologic imaging with positron emission tomography. Curr Top Med Chem. 2013; 13:871–891. [PubMed: 23590170]
16. Cho SY, Gage KL, Mease RC, et al. Biodistribution, tumor detection, and radiation dosimetry of 18F-DCFBC, a low-molecular-weight inhibitor of prostate-specific membrane antigen, in patients with metastatic prostate cancer. J Nucl Med. 2012; 53:1883–1891. [PubMed: 23203246]
17. Szabo Z, Mena E, Rowe SP, et al. Initial evaluation of [18F]DCFPyL for prostate-specific membrane antigen (PSMA)-targeted PET imaging of prostate cancer. Mol Imaging Biol. 2015; 17:565–574. [PubMed: 25896814]
18. Afshar-Oromieh A, Malcher A, Eder M, et al. PET imaging with a [68Ga]gallium-labelled PSMA ligand for the diagnosis of prostate cancer: biodistribution in humans and first evaluation of tumour lesions. Eur J Nucl Med Mol Imaging. 2013; 40:486–495. [PubMed: 23179945]
19. Viola-Villegas NT, Sevak KK, Carlin SD, et al. Noninvasive imaging of PSMA in prostate tumors with (89)Zr-labeled huJ591 engineered antibody fragments: the faster alternatives. Mol Pharm. 2014; 11:3965–3973. [PubMed: 24779727]
20. Osborne JR, Green DA, Spratt DE, et al. A prospective pilot study of (89)Zr-J591/prostate specific membrane antigen positron emission tomography in men with localized prostate cancer undergoing radical prostatectomy. J Urol. 2014; 191:1439–1445. [PubMed: 24135437]
21. Pandit-Taskar N, O'Donoghue JA, Beylergil V, et al. (8)(9) ZrhuJ591 immuno-PET imaging in patients with advanced metastatic prostate cancer. Eur J Nucl Med Mol Imaging. 2014; 41:2093–2105. [PubMed: 25143071]
22. Afshar-Oromieh A, Hetzheim H, Kratochwil C, et al. The novel theranostic PSMA-ligand PSMA-617 in the diagnosis of prostate cancer by PET/CT: biodistribution in humans, radiation dosimetry and first evaluation of tumor lesions. J Nucl Med. 2015; 56:1697–1705. [PubMed: 26294298]
23. Foss CA, Mease RC, Cho SY, Kim HJ, Pomper MG. GCPII imaging and cancer. Curr Med Chem. 2012; 19:1346–1359. [PubMed: 22304713]
24. Chang SS. Overview of prostate-specific membrane antigen. Rev Urol. 2004; 6(Suppl 10):S13–S18.
25. Wright GL Jr, Grob BM, Haley C, et al. Upregulation of prostate-specific membrane antigen after androgen-deprivation therapy. Urology. 1996; 48:326–334. [PubMed: 8753752]
26. Evans MJ, Smith-Jones PM, Wongvipat J, et al. Noninvasive measurement of androgen receptor signaling with a positron-emitting radiopharmaceutical that targets prostate-specific membrane antigen. Proc Natl Acad Sci U S A. 2011; 108:9578–9582. [PubMed: 21606347]
27. Noss KR, Wolfe SA, Grimes SR. Upregulation of prostate specific membrane antigen/folate hydrolase transcription by an enhancer. Gene. 2002; 285:247–256. [PubMed: 12039052]
28. Perner S, Hofer MD, Kim R, et al. Prostate-specific membrane antigen expression as a predictor of prostate cancer progression. Hum Pathol. 2007; 38:696–701. [PubMed: 17320151]
29. Ross JS, Sheehan CE, Fisher HA, et al. Correlation of primary tumor prostate-specific membrane antigen expression with disease recurrence in prostate cancer. Clin Cancer Res. 2003; 9:6357–6362. [PubMed: 14695135]
30. Rowe SP, Gage KL, Faraj SF, et al. 18F-DCFBC PET/CT for PSMA-based detection and characterization of primary prostate cancer. J Nucl Med. 2015; 56:1003–1010. [PubMed: 26069305]
31. Rowe SP, Macura KJ, Ciarallo A, et al. Comparison of prostate-specific membrane antigen-based 18F-DCFBC PET/CT to conventional imaging modalities for detection of hormone-naïve and castration-resistant metastatic prostate cancer. J Nucl Med. 2016; 56:46–53.
32. Chen Y, Pullambhatla M, Foss CA, et al. 2-(3-{1-Carboxy-5-[(6-[18F]fluoro-pyridine-3-carbonyl)-amino]-pentyl}-ureido)-pen tanedioic acid, [18F]DCFPyL, a PSMA-based PET imaging agent for prostate cancer. Clin Cancer Res. 2011; 17:7645–7653. [PubMed: 22042970]

33. Yao V, Berkman CE, Choi JK, O'Keefe DS, Bacich DJ. Expression of prostate-specific membrane antigen (PSMA), increases cell folate uptake and proliferation and suggests a novel role for PSMA in the uptake of the non-polyglutamated folate, folic acid. Prostate. 2010; 70:305–316. [PubMed: 19830782]

34. Yao V, Parwani A, Maier C, Heston WD, Bacich DJ. Moderate expression of prostate-specific membrane antigen, a tissue differentiation antigen and folate hydrolase, facilitates prostate carcinogenesis. Cancer Res. 2008; 68:9070–9077. [PubMed: 18974153]

35. Team RC. R: a language and environment for statistical computing. R Foundation for Statistical Computing; Vienna: 2014.

36. Liang K-Y, Scott Z. Longitudinal data analysis using generalized linear models. Biometrika. 1986; 73:13–22.

37. Eiber M, Maurer T, Souvatzoglou M, et al. Evaluation of hybrid 68Ga-PSMA Ligand PET/CT in 248 patients with biochemical recurrence after radical prostatectomy. J Nucl Med. 2015; 56:668–674. [PubMed: 25791990]

38. Morigi JJ, Stricker PD, van Leeuwen PJ, et al. Prospective comparison of 18F-fluoromethylcholine versus 68Ga-PSMA PET/CT in prostate cancer patients who have rising PSA after curative treatment and are being considered for targeted therapy. J Nucl Med. 2015; 56:1185–1190. [PubMed: 26112024]

39. Afshar-Oromieh A, Zechmann CM, Malcher A, et al. Comparison of PET imaging with a (68)Ga-labelled PSMA ligand and (18)F-choline-based PET/CT for the diagnosis of recurrent prostate cancer. Eur J Nucl Med Mol Imaging. 2014; 41:11–20. [PubMed: 24072344]

40. Dietlein M, Kobe C, Kuhnert G, et al. Comparison of [F]DCFPyL and [Ga]Ga-PSMA-HBED-CC for PSMA-PET imaging in patients with relapsed prostate cancer. Mol Imaging Biol. 2015; 17:575–584. [PubMed: 26013479]

41. Sanchez-Crespo A. Comparison of gallium-68 and fluorine-18 imaging characteristics in positron emission tomography. Appl Radiat Isot. 2013; 76:55–62. Including data, instrumentation and methods for use in agriculture, industry and medicine. [PubMed: 23063597]

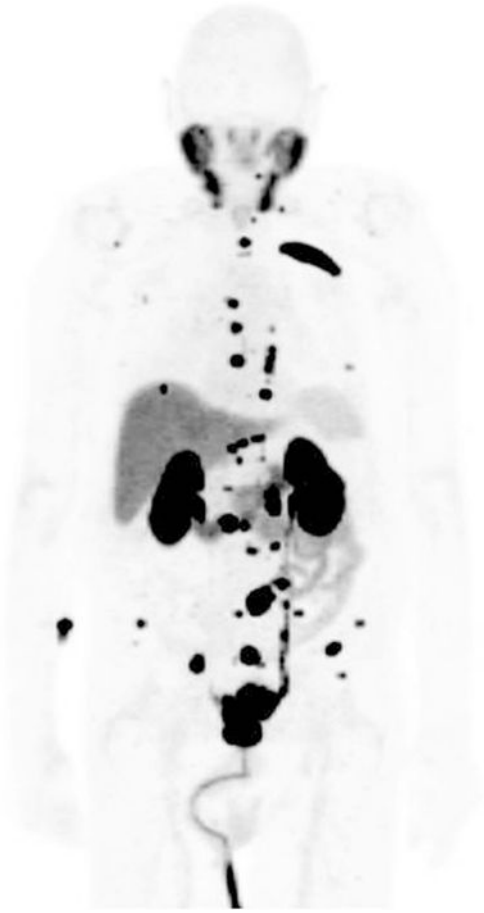

Fig. 1.

Whole body MIP image of a patient with numerous sites of [^{18}F]DCFPyL PET positive bone and lymph node lesions, most likely representing sites of prostate cancer metastases.

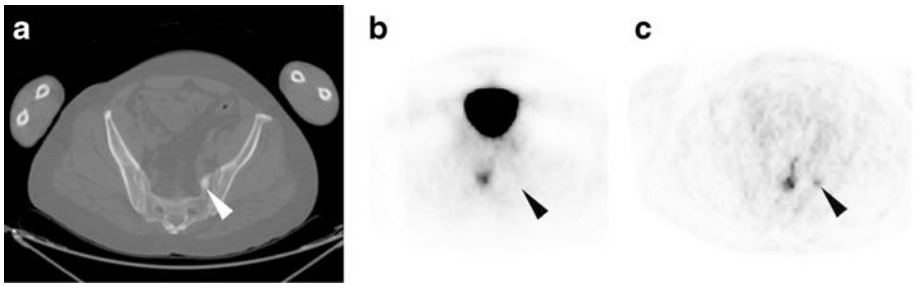

Fig. 2.

a CT; **b** PET4; and **c** PET5 images from a patient with a sclerotic bone lesion in the left sacrum (*arrowheads*). There is no appreciable [^{18}F]DCFPyL uptake at the PET4 time point, with interval detection of focal mild but positive uptake on PET5. Intense urinary activity within the bladder seen on PET4 is not seen on PET5 secondary to patient voiding.

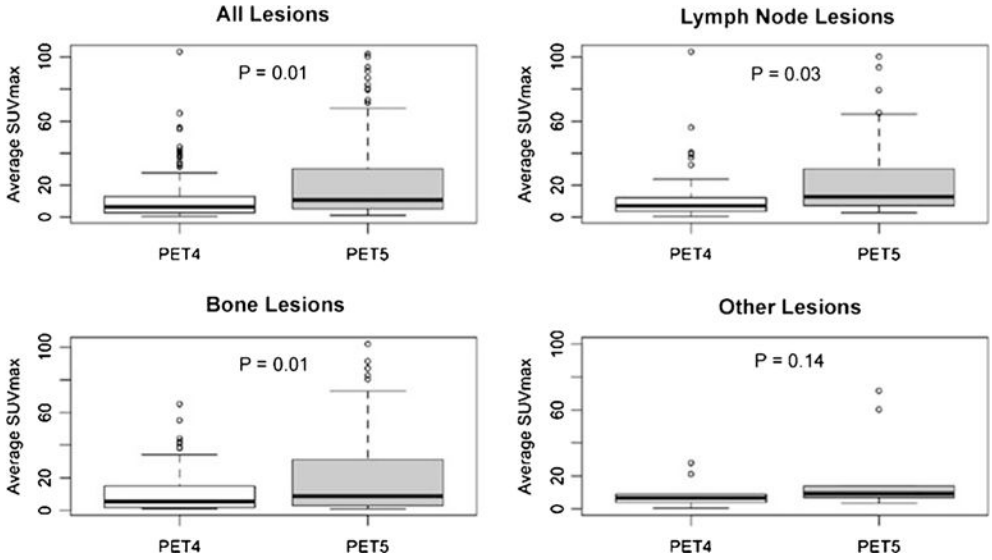

Fig. 3.

Box plot of average tumor SUV_{max} at the PET4 and PET5 time points (~60 and at 120 min post-injection, respectively) for all, bone, lymph node, and other sites.

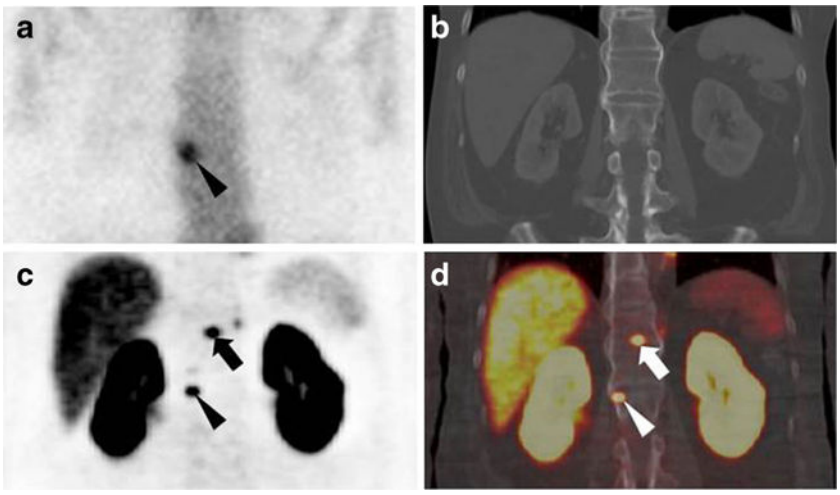

Fig. 4.

a Anterior planar BS; **b** coronal CECT; **c** coronal [^{18}F]DCFPyL PET; and **d** coronal [^{18}F]DCFPyL PET/CT images from a patient with multiple sites of presumed metastatic disease. Uptake in the left anterior L2 vertebral body (*arrowheads*) is clearly visible on [^{18}F]DCFPyL PET and BS but occult on CT. An additional site of uptake seen on [^{18}F]DCFPyL PET in T12 vertebral body (*arrows*) is not seen on BS or CECT. Of note, there is also subtle [^{18}F]DCFPyL PET uptake also seen in L1 and in a small retrocrural lymph node.

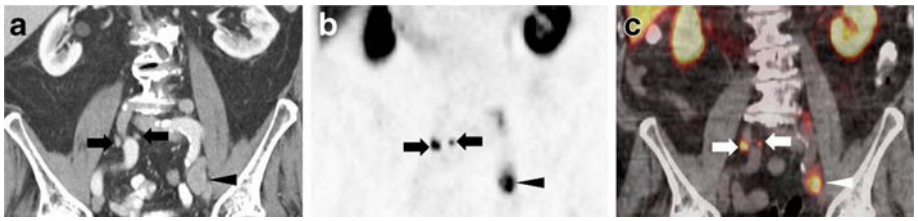

Fig. 5.

a Coronal CECT; **b** coronal [^{18}F]DCFPyL PET; and **c** coronal [^{18}F]DCFPyL fused PET/CT images of a patient with multiple lymph node lesions. There is a large (2.0 cm short axis) lymph node near the region of the bifurcation of the left common iliac artery (*arrowheads*) that demonstrates intense [^{18}F]DCFPyL PET uptake. Additionally, small (4 and 6 mm short axis) lymph nodes in the right common iliac chain (*arrows*) are also intensely [^{18}F]DCFPyL-avid.

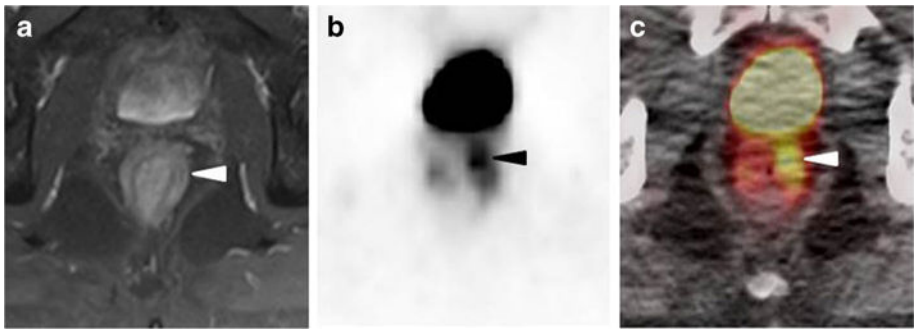

Fig. 6.

a Axial T2 MRI with endo-rectal probe; **b** axial [^{18}F]DCFPyL PET; and **c** axial [^{18}F]DCFPyL fused PET/CT images of the rectal and peri-rectal tissues in a patient with suspected metastatic prostate cancer. Asymmetric radiotracer uptake in the left anterior soft tissues within or adjacent to the rectal wall can be seen (*arrowheads*) without a corresponding finding on the MRI. This was found to be a site of metastatic prostate cancer on biopsy.

Table 1

Selected demographic and clinical information on the patients included in this trial

Patient	Age	Gleason	PSA (ng/ml)	Current therapy
1	67	9	8.6	None
2	62	7	6.0	None
3	51	9	0.1	Androgen deprivation therapy
4	85	7	26.2	None
5	88	7	5.1	None
6	73	9	8.0	Enzalutamide
7	63	7	11.0	Androgen deprivation therapy
8	73	9	204.8	Sipuleucel-T
9	77	10	5.3	Enzalutamide

Table 2

Number of lesions detected with each modality by lesion type. Lesions were categorized as either definite or equivocal by the central reviewers

Modality	All lesions		Bone lesions		Lymph node lesions		Other lesions[a]	
	Definite	Equivocal	Definite	Equivocal	Definite	Equivocal	Definite	Equivocal
[^{18}F]DCFPyL PET	138	1	73	1	56	0	9	0
CECT	20	11	8	9	7	0	5	2
BS	13	5	13	5	N/A	N/A	N/A	N/A
Combined CIM	30	15	18	13	7	0	5	2

CECT contrast-enhanced CT, *BS* bone scan, *CIM* conventional imaging modalities (CECT + BS)

[a]Other lesions includes prostate, prostate bed, peri-prostatic tissue, and other soft tissue sites

Mol Imaging Biol. Author manuscript; available in PMC 2017 January 24.

Table 3

Estimated proportions of inter-modality agreement for detection of metastatic disease accounting for intra-patient correlation using GEE regression analysis

Modality	All lesions (95 % CI)	Bone (95 % CI)	Lymph node (95 % CI)	Other lesions[a] (95 % CI)
Positive on [^{18}F]DCFPyL PET, negative or equivocal on CECT	0.59 (0.38–0.77)	0.49 (0.24–0.74)	0.83 (0.64–0.93)	0.39 (0.16–0.68)
Positive on [^{18}F]DCFPyL PET, negative or equivocal on BS	0.77 (0.62–0.88)	0.37 (0.16–0.65)	N/A	N/A
Positive on [^{18}F]DCFPyL PET, negative or equivocal on CIM	0.54 (0.34–0.72)	0.28 (0.09–0.60)	0.83 (0.64–0.93)	0.39 (0.16–0.68)
Positive on CECT, negative or equivocal on [^{18}F]DCFPyL PET	0.03 (0.01–0.08)	0.05 (0.03–0.10)	0.00 (0.00–0.00)	0.00 (0.00–0.00)
Positive on BS, negative or equivocal on [^{18}F]DCFPyL PET	0.01 (0.00–0.05)	0.02 (0.00–0.13)	N/A	N/A
Positive on CIM, negative or equivocal on [^{18}F]DCFPyL PET	0.03 (0.01–0.08)	0.07 (0.02–0.17)	0.00 (0.00–0.00)	0.00 (0.00–0.00)

The corresponding 95 % confidence intervals are in parentheses

CECT contrast-enhanced CT, *BS* bone scan, *CIM* conventional imaging modalities (CECT + BS)

[a] Other lesions includes prostate, prostate bed, peri-prostatic tissue, and other soft tissue sites